A. Mathematical model of water electrolysis

A proton exchange membrane electrolysis cell (PEMEC) is used to convert electricity to hydrogen because of its fast startup–shutdown capability and the potential for efficiency improvement and cost reduction [1]. The main assumptions underlying the model in this study serve to realise a good compromise between accuracy and complexity. The following assumptions were made:

- The stack model reduces to identical PEMECs connected in series [2].
- The temperature is uniform in the electrolyser stack [2].
- The only gaseous products present at the anode are oxygen and water vapour, whereas the only gaseous products at the cathode are hydrogen and water vapour [2].
- The diffusion of hydrogen and oxygen through the membrane is negligible because the diffusion rate is relatively low [3].

When a PEMEC operates, an input voltage is applied to the electrodes, and several voltage drops appear owing to fundamental overpotential [4]. The first term in (A.2) is the reversible cell voltage U^{rev}, which is the theoretical voltage required by the electrolyser. The ohmic overvoltage U^{ohm} is due to the resistance to the electron flow through the current collectors and separator plates, as well as the resistance to the conduction of protons through the membrane. The activation overvoltage U^{act} is due to the electronic resistance and the resistance to the flow of electrons. The operating voltage is the sum of all overvoltages, as shown in (A.2) [4]. Eq. (A.6) is the relationship between the operating current and current density [5]. The hydrogen production and oxygen production are determined by (A.7), respectively [5]. The corresponding technical parameters are listed in Table A1.

$$\dot{P}_t^{\text{WE}} = U_t^{\text{cell}} I_t^{\text{cell}}, \forall t \tag{A.1}$$

$$U_t^{\text{cell}} = U_t^{\text{rev}}(T_t^{\text{cell}}) + U_t^{\text{ohm}}(i^{\text{cell}}, T_t^{\text{cell}}) + U_t^{\text{act}}(i^{\text{cell}}, T_t^{\text{cell}}), \forall t \tag{A.2}$$

$$\begin{aligned} U_t^{\text{rev}}(T_t^{\text{cell}}) &= U^{\text{rev}_0}(T_t^{\text{cell}}) + \frac{RT_t^{\text{cell}}}{2F} \ln\left(\frac{p^{\text{H}_2} p^{\text{O}_2 0.5}}{a^{\text{H}_2\text{O}}}\right), \forall t \\ U_t^{\text{rev}_0}(T_0^{\text{cell}}) &= 1.229 - 0.9 \times 10^{-3}(T_t^{\text{cell}} - 298), \forall t \end{aligned} \tag{A.3}$$

$$U_t^{\text{ohm}}(i^{\text{cell}}, T_t^{\text{cell}}) = i_t^{\text{cell}} R^{\text{cell}}(T_t^{\text{cell}}), \forall t \tag{A.4}$$

$$U_t^{\text{act}}(i^{\text{cell}}, T_t^{\text{cell}}) = \frac{RT^{\text{cell}}}{\alpha^{\text{an}} F} arsinh\left(\frac{i_t^{\text{cell}}}{2i^{\text{an}}}\right) + \frac{RT_t^{\text{cell}}}{\alpha^{\text{cat}} F} arsinh\left(\frac{i_t^{\text{cell}}}{2i^{\text{cat}}}\right), \forall t \tag{A.5}$$

$$I_{i,t}^{\text{cell}} = A^{\text{cell}} i_t^{\text{cell}}, \forall t \tag{A.6}$$

$$\dot{m}_t^2 = \frac{N^{\text{cell}} I_t^{\text{cell}} h^{\text{F}}}{2F}, \dot{m}_t^4 = \frac{N^{\text{cell}} I_t^{\text{cell}} h^{\text{F}}}{4F}, \forall t \tag{A.7}$$

Table A1 Technical parameters of the proton-exchange membrane electrolyser.

Parameter	Value	Reference
Hydrogen product pressure p^{H_2}	20 bar	[6]
Oxygen outlet pressure p^{O_2}	1.013 bar	[6]
Anode exchange current density i^{an}	1.7e-6 A/cm^2	[6]
Cathode exchange current density i^{cat}	1e-3 A/cm^2	[6]
Anode charge transfer coefficient α^{an}	2	[1]
Cathode charge transfer coefficient α^{cat}	0.5	[1]
Active cell area A^{cell}	1000 cm^2	[6]
water activity $a^{\text{H}_2\text{O}}$	1	[1]
Faraday constant F	96487 C/mol	[6]
Faraday's efficiency h^{F}	99%	[6]
Ideal gas constant R	8.314 J/mol·K	[6]
unit conversion factor	1e-6 (W→MW)	-
unit conversion factor	0.0225 (mol/s→Nm^3/s)	-

The current density-dependent cell voltage contributions are derived in the Fig. A1. The blue line is the I-U curve obtained from the model in this paper, and the blue area is the I-U curve obtained from the statistics in Fig.7 of the literature [6], which can be seen that the model in this paper yields the range of data published in the review literature [7].

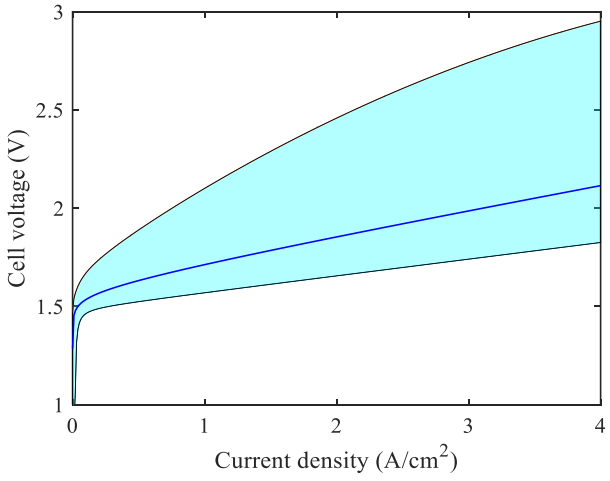

Fig. A1 I-U-curves of PEM electrolysis.

B. Mathematical model of biomass gasification

The gasification process includes drying, pyrolysis, combustion, and reduction. Downdraft gasifiers can be classified into two types: throat and open-core. The former is considered in the present work and is suitable for biomass fuels with low ash content and uniform size [8]. The gasifying agent is supplied to the gasifier to react with the solid fuel during the combustion step. An increase in the oxygen concentration of the gasifying agent enhances the hydrogen concentration and energy efficiency [8].

A thermodynamic model is used to calculate the product gas composition during the gasification [9]. It is assumed that all reactions are in equilibrium and that the pyrolysis product burns and reaches equilibrium in the reduction zone before leaving the gasifier [10]. In addition, the following assumptions are made in the analysis of biomass gasification:

- The system works under steady state conditions [11].
- The changes in the kinetic and potential energies and exergies are negligible because they are very small compared to the changes in the corresponding thermal values [11].
- The ash residue from the gasification process is negligible because the ash content of biomass fuels is typically very low [10].
- The downdraft gasifier produces a very small amount of tar which is neglected in this model [8].
- As can be verified by reference to the appropriate property data, the gas mixtures behave as ideal gases in the states under consideration [11].
- The producer gas leaves the gasifier at the gasifier temperature as thermodynamic equilibrium model is considered [8].
- The formation of NO_X is not considered because of the very small amount of NO_X generated [8].

The input data used to model the gasification process are listed in Table B1.

Table B1 Input data for the gasification process modelling.

Parameter	Value	Reference
Air inlet temperature	298 K	[8]
Biomass inlet temperature	298 K	[8]
Temperature of syngas exiting gasifier	1023 K	[12]
Environmental temperature	298 K	[8]
Moisture content in biomass	10%	[12]
Molar composition of environmental air	21%O_2, 79%N_2	[12]

For biomass gasification process with oxygen, the global gasification reaction is as follows:

$$CH_xO_y + wH_2O + c^{O_2\_BG}O_2 = c^{H_2\_BG}H_2 + c^{CO\_BG}CO + c^{CO_2\_BG}CO_2 + c^{H_2O\_BG}H_2O + c^{CH_4\_BG}CH_4 \quad \text{(B.1)}$$

where CH_xO_y shows the biomass as the feedstock, w represents the biomass moisture content and $c^{O_2\_BG}$ is the number of moles of oxygen per mole of the biomass material. $c^{H_2\_BG}$ to $c^{CH_4\_BG}$ are the stoichiometric coefficients of constituents of the product that are determined by writing element balances for H, C and O.

The relationship between biomass, oxygen, and produced gas can be obtained based on the element balance, equilibrium constant, and heat balance.

The moisture content per mole of biomass is calculated from the following equation:

$$w = \frac{MW_{biomass} \times MC}{MW_w \times (1 - MC)} \quad \text{(B.2)}$$

where $MW_{biomass}$ and MW_w demonstrate the biomass and water molecular weights, respectively. MC is the moisture content of biomass.

The element balances of carbon, hydrogen and oxygen for the global reaction are as below:

Carbon balance:

$$c^{CO\_BG} + c^{CO_2\_BG} + c^{CH_4\_BG} = 1 \quad \text{(B.3)}$$

Hydrogen balance:

$$2c^{H_2\_BG} + 2c^{H_2O\_BG} + 4c^{CH_4\_BG} = 2w + a \quad \text{(B.4)}$$

Oxygen balance:

$$c^{CO\_BG} + 2c^{CO_2\_BG} + c^{H_2O\_BG} = 2c^{O_2\_BG} + w + b \quad \text{(B.5)}$$

The chemical reactions occurring in the gasification process in the presence of air are given by:

$$C + 2H_2 \leftrightarrow CH_4 \qquad \Delta H = -75 \text{ kJ/mol} \quad \text{(B.6)}$$

$$CO_2 + H_2 \rightarrow CO + H_2O \qquad \Delta H = 41.2 \text{ kJ/mol} \quad \text{(B.7)}$$

The equilibrium constant (K_i) for methane generation (Eq. B.6) and for water-gas reaction (Eq. B.7) can be expressed based on the participating species in stoichiometric coefficient as below:

$$K_1 = \frac{c^{CH_4\_BG}}{(c^{H_2\_BG})^2} \cdot \frac{1}{(x_t)} \quad \text{(B.8)}$$

$$K_2 = \frac{c^{CO_2\_BG} c^{H_2\_BG}}{c^{CO\_BG} c^{H_2O\_BG}} \quad \text{(B.9)}$$

where x_t is the total number of produced gas.

On the other hand, the equilibrium constants as a function of temperature are expressed as follows:

$$\ln K_1 = \frac{7082.848}{T} + (-6.567)\ln T + \frac{7.466\times10^{-3}}{2}T + \frac{-2.164\times10^{-6}}{6}T^2 + \frac{0.701\times10^{-5}}{2(T)^2} + 32.541 \quad \text{(B.10)}$$

$$\ln K_2 = \frac{5870.53}{T} + 1.86\ln T - 2.7\times10^{-4}T + \frac{58200}{T^2} - 18.007 \quad \text{(B.11)}$$

The energy balance is the last necessary equation for the model, which can be written as below:

$$h^0_{f,biomass} + wh_{H_2O} + c^{O_2\_BG}h_{O_2} = c^{H_2\_BG}h_{H_2} + c^{CO\_BG}h_{CO} + c^{CO_2\_BG}h_{CO_2} + c^{H_2O\_BG}h_{H_2O} + c^{CH_4\_BG}h_{CH_4} + Q_{lost} \quad \text{(B.12)}$$

where h is enthalpy of components given by the following equation, Q_{lost} is the heat injection from the gasifier wall.

The component percentages of the producer gas obtained from the present study for each gasification agent are compared with those reported previously in Table B2. These comparisons show that the results obtained from the proposed model agree well with those reported in the literature.

Table B2 Component percentages in the producer gas under air and oxygen gasifying agent (Biomass: wood)

Research	Gasifying agent	Hydrogen	Methane	Carbon monoxide	Carbon dioxide	Nitrogen
Experimental results [14]	Air	15.23	1.58	23.04	16.42	42.31
Experimental results [13]	95% O_2, 5% N_2	32	2	48	15	3
Equilibrium model [12]	Air	21.66	1.01	25.55	9.36	44.42
Equilibrium model [8]	95% O_2, 5% N_2	37.5	3.09	45.6	12.98	0.03
Present work	Air	21.87	1.07	25.25	10.23	41.58
Present work	100% O_2	39.67	2.60	45.05	12.68	0

C. Mathematical model of natural gas reforming

In Fig. C1, the chemical-looping auto-thermal reforming (CLRa) process consists of two interconnected reactors designated as fuel and steam reactors. The oxygen carrier in the fuel reactor is reduced to a low-valence oxide (MeO_n) or a simple substance (Me), and generates H_2O and CO_2, which can be directly captured and sequestered after H_2O condensation. In the steam reactor, MeO_n or Me is partially oxidised by H_2O, and the produced gas is condensed to obtain high-purity H_2. In addition, the reduced oxygen carrier is completely oxidized by oxygen (O_2), and a large amount of heat is released to maintain the heat balance of the system. In addition, methane (CH_4) is used as fuel, and ferric oxide is used as oxygen carrier.

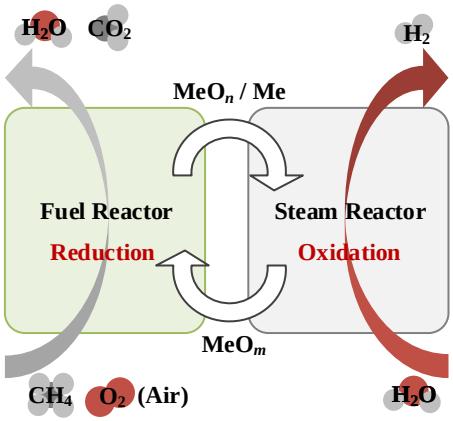

Fig. C1 Chemical-looping auto-thermal reforming process.

The CLRa model is based on mass and heat balance and does not consider the kinetics of the reaction [15]. The input data used to model the reforming process are listed in Table C1. The main assumptions used for the calculations are as follows:

- Gas fuel fed to the fuel reactor is CH_4 [16].
- Temperature in the fuel reactor is kept constant [16].
- Inlet gases are heated with the sensible-heat of the gas outlet streams of biomass gasification.
- In the fuel reactor a complete CH_4 conversion has been assumed [17].
- There are no heat losses in the reactors [16].
- The simulation is carried outperformed based on the stable state, and the fuel reactor and steam reactors are assumed to be in an adiabatic state [18].

Table C1 Input data to model the CLRa process.

Parameter	Value	Reference
Fuel reactor temperature	1200 K	[16]
Conversions of the oxygen-carrier at the exit of the steam X^{SR}	1	[16]
Oxygen carrier circulation flow rate N^s	0.2-10.2 kg/s	[17]
Environmental temperature	298 K	[18]
Reactors operating pressures	12 bar	[18]
Inlet CH_4	1 mol/s	[16]
Molar composition of environmental air	21%O_2, 79%N_2	[18]

Eqs. (C.1) and (C.2) represent the mass balance equations of the fuel and steam reactors, respectively [16]. Enthalpy of reactants H^{re}, products H^{pr} and enthalpy change ΔH form the heat balance equation in (C.3) [15]. When $\Delta H = 0$, the system reaches CLRa state. Enthalpy of reactants H^{re} and products H^{pr} can be calculated by (C.4) [15]. The enthalpy of gas h_j is related to the gas temperature T^{gas}, which can be calculated by (C.5) [16].

$$\frac{N^s y^{Fe_3O_4\_ox}}{M^{Fe_3O_4}} \Delta X^s = N^{FeO} + N^{Fe}, \Delta X^s = X^{SR} - X^{FR} \tag{C.1}$$

$$\frac{N^s y^{Fe_3O_4\_ox}}{M^{Fe_3O_4}} X^{SR} = N^{Fe_3O_4} \tag{C.2}$$

$$H^{re} = H^{pr} - \Delta H \tag{C.3}$$

$$H^{re} = \sum N_j^{re\_gas} h_j^{re\_gas}, H^{pr} = \sum N_j^{pr\_gas} h_j^{pr\_gas} \tag{C.4}$$

$$h_j = h_{0j} + \int_{298}^{T^{gas}} C_{pj}(T^{gas}) dT^{gas} \tag{C.5}$$

where $y^{Fe_3O_4-ox}$ is the fraction of Fe_3O_4 in the oxygen carrier when it is completely oxidised; $M^{Fe_3O_4}$ is the molecular weight of Fe_3O_4; X^{SR} and X^{FR} are the conversions of the oxygen-carrier at the exit of the steam and fuel reactors, respectively; N^{Fe}, N^{FeO}, and $N^{Fe_3O_4}$ is the molar flows of Fe, FeO, and Fe_3O_4; h_{0j} is the enthalpy of component j at 298 K, which is available in Barin's handbook on pure substance thermochemistry [19]; and C_{pj} is the heat capacity of component j, which is referred to [19].

The products (N^{pr_gas}) can be calculated from the above model. The results are first compared with the thermodynamic analyses in [17] to validate the model presented in Table C2.

Table C2 Component percentage in the producer gas of CLRa

Research	Reactor	Hydrogen	Carbon monoxide	Water vapor	Oxygen
Thermodynamic analyses [17]	Steam reactor	50	0	50	0
	Fuel reactor	0	36.37	63.46	0
Present work	Steam reactor	50	33.33	66.67	0
	Fuel reactor	0	45.05	12.68	0

References

[1] Carmo M, Fritz D L, Mergel J, et al. A comprehensive review on PEM water electrolysis. International journal of hydrogen energy, 2013, 38(12): 4901-4934. https://doi.org/10.1016/j.ijhydene.2013.01.151.

[2] García-Valverde R, Espinosa N, Urbina A. Simple PEM water electrolyser model and experimental validation. international journal of hydrogen energy, 2012, 37(2): 1927-1938. https://doi.org/10.1016/j.ijhydene.2011.09.027.

[3] Biaku C Y, Dale N V, Mann M D, et al. A semiempirical study of the temperature dependence of the anode charge transfer coefficient of a 6 kW PEM electrolyzer. International journal of hydrogen energy, 2008, 33(16): 4247-4254. https://doi.org/10.1016/j.ijhydene.2008.06.006.

[4] Awasthi A, Scott K, Basu S. Dynamic modeling and simulation of a proton exchange membrane electrolyzer for hydrogen production. International journal of hydrogen energy, 2011, 36(22): 14779-14786. https://doi.org/10.1016/j.ijhydene.2011.03.045.

[5] Görgün H. Dynamic modelling of a proton exchange membrane (PEM) electrolyzer. International journal of hydrogen energy, 2006, 31(1): 29-38. https://doi.org/10.1016/j.ijhydene.2005.04.001.

[6] Hemauer J, Rehfeldt S, Klein H, et al. Performance and cost modelling taking into account the uncertainties and sensitivities of current and next-generation PEM water electrolysis technology. International Journal of Hydrogen Energy, 2023. https://doi.org/10.1016/j.ijhydene.2023.03.050.

[7] Buttler A, Spliethoff H. Current status of water electrolysis for energy storage, grid balancing and sector coupling via power-to-gas and power-to-liquids: A review. Renewable and Sustainable Energy Reviews, 2018, 82: 2440-2454. https://doi.org/10.1016/j.rser.2017.09.003.

[8] Shayan E, Zare V, Mirzaee I. Hydrogen production from biomass gasification; a theoretical comparison of using different gasification agents. Energy Conversion and management, 2018, 159: 30-41. https://doi.org/10.1016/j.enconman.2017.12.096.

[9] Samimi F, Marzoughi T, Rahimpour M R. Energy and exergy analysis and optimization of biomass gasification process for hydrogen production (based on air, steam and air/steam gasifying agents). International Journal of Hydrogen Energy, 2020, 45(58): 33185-33197. https://doi.org/10.1016/j.ijhydene.2020.09.131.

[10] Sansaniwal S K, Pal K, Rosen M A, et al. Recent advances in the development of biomass gasification

technology: A comprehensive review. Renewable and sustainable energy reviews, 2017, 72: 363-384. https://doi.org/10.1016/j.rser.2017.01.038.

[11] Colpan C O, Hamdullahpur F, Dincer I, et al. Effect of gasification agent on the performance of solid oxide fuel cell and biomass gasification systems. International Journal of Hydrogen Energy, 2010, 35(10): 5001-5009. https://doi.org/10.1016/j.ijhydene.2009.08.083.

[12] Zainal Z A, Ali R, Lean C H, et al. Prediction of performance of a downdraft gasifier using equilibrium modeling for different biomass materials. Energy conversion and management, 2001, 42(12): 1499-1515. https://doi.org/10.1016/S0196-8904(00)00078-9.

[13] Alauddin Z A Z. Performance and characteristics of a biomass gasifier system. University of Wales, Cardiff, 1996.

[14] La Villetta M, Costa M, Massarotti N. Modelling approaches to biomass gasification: A review with emphasis on the stoichiometric method. Renewable and Sustainable Energy Reviews, 2017, 74: 71-88. https://doi.org/10.1016/j.rser.2017.02.027.

[15] Kang K S, Kim C H, Bae K K, et al. Oxygen-carrier selection and thermal analysis of the chemical-looping process for hydrogen production. International Journal of Hydrogen Energy, 2010, 35(22): 12246-12254. https://doi.org/10.1016/j.ijhydene.2010.08.043.

[16] Ortiz M, Abad A, De Diego L F, et al. Optimization of hydrogen production by chemical-looping auto-thermal reforming working with Ni-based oxygen-carriers. International Journal of Hydrogen Energy, 2011, 36(16): 9663-9672. https://doi.org/10.1016/j.ijhydene.2011.05.025.

[17] Chiesa P, Lozza G, Malandrino A, et al. Three-reactors chemical looping process for hydrogen production[J]. International journal of hydrogen energy, 2008, 33(9): 2233-2245. https://doi.org/10.1016/j.ijhydene.2008.02.032.

[18] Zhang Y, Kong F, Tong A, et al. Autothermal operation strategies of chemical looping processes for hydrogen generation: process simulation, parametric studies, and exergy analysis. Industrial & Engineering Chemistry Research, 2020, 59(13): 5877-5890. https://doi.org/10.1021/acs.iecr.9b06130.

[19] Barin I, Platzki G. Thermochemical data of pure substances. Weinheim: VCh, 1989. https://doi.org/10.1002/9783527619825.